An Empirical Channel Model for the Effect of Human Body on Ray Tracing

Yishuang Geng*, Yadong Wan†, Jie He† and Kaveh Pahlavan*
*Center for Wireless and Information Network Studies (CWINS)
Worcester Polytechnic Institute (WPI), Worcester, Massachusetts 01609, USA
†School of Computer and Communication Engineering
University of Science and Technology Beijing (USTB), Beijing, 100083, China
Email: *{ygeng and kaveh}@wpi.edu, †{yadong.wan and hejie1983}@gmail.com

***Abstract*—This paper presents a empirical model for near human body UWB propagation channel that is valid for the frequency range from 3GHz to 8GHz. It is based on measurements conducted in a anechoic chamber which can be regarded as free space. The empirical model shows the joint propagation characteristics of the on body channel and the channel between body surface and external access point. It includes the loss of the first path, arrival time of the first path and the total pathloss. Models for all three aspects have been partitioned into two sections by a break point due to the geometrical property of human body and the creeping wave phenomenon. The investigation on first path behavior can be regarded as a theoretical basis of ray-tracing technique that takes the effects of human body into consideration.**

I. Introduction

The mergence of wireless body area networks (WBAN) and wireless local area networks (WLAN) are finding an increasing number of applications in indoor environment such as health monitoring, indoor human tracking and etc. and such rapid expansion results in significant advances in the development of wireless access and localization. Since the ultimate performance of these applications is limited by the wireless channel they operate in, researches on propagation characteristics received much attention in the recent years [1]. Among the available spectrum resources, ultra-wideband (UWB) is one of the most promising candidate for these indoor applications due to its fading tolerance, lower interference and easier penetration on the communication aspect as well as the high accuracy property on the localization aspect.

A number of traditional statistical UWB channel models for indoor environment have been posted in the literature. [1] proposed a wide band channel model which is later on adopted by IEEE 802.15.4a for low frequency UWB system evaluation. [2] is adopted by the IEEE 802.15.3a group as the standard UWB channel model for frequency ranging from 3GHz to 10GHz. In the latest IEEE 802.15.6 standard for body area networks, UWB models are also developed for the channel from body surface to body surface (CM3) and from body surface to external access point (CM4) [3]. Such statistical models are easy-to-use and computationally efficient in general, but they suffer the lack of accuracy due to the fact that statistical models are derived from extensive measurement results which are not specific to the intended deployment environment [4].

To avoid the costly and time consuming field measurement, the most popular method to come up with the site-specific propagation characteristics is ray-tracing [5]. Ray-tracing technique is an approach that can obtain channel characteristic by identifying the contributions of individual multipath component and calculating their composition at the receiver. Since each individual multipath component is described in terms of rays, optical effects such as absorption, reflection and diffraction of surrounding walls and stuff that make up the indoor environment can be taken into account. As for BAN applications, human body itself also has a strong influence on the waveform propagation and it can be regarded as a special and complex obstacle to the passing rays. However, no ray-tracing model considering human body can be found in the open literature until now.

Related researches reported that the over 80 dB penetration loss eliminates the direct path that penetrate the human body and the radio frequency (RF) signal get scattered on the surface of human body and travels in the pattern of creeping wave [6] [7]. As is mentioned before, the IEEE 802.15.6 group developed pathloss model for CM3 and CM4. However, these given channel models are not adequate to design ray-tracing model considering human body for the following reasons: 1) When passing the human body, the behavior of creeping wave should be modeled as a function of both distance and incidence angle. 2) The behavior of creeping wave should be modeled as the joint propagation characteristics of CM3 and CM4. 3) Apart from the total pathloss, power of each individual path is also critical in designing ray-tracing technology.

In this paper, measurements have been conducted inside an anechoic chamber with the transmitter (Tx) mounted to the chest of human body and receiver (Rx) located in the surrounding area with different distance to Tx and different incidence angle. Based on the empirical measurement result, the pathloss of the first path has been modeled to be partitioned into two sections by the break point. The break point is modeled as a function of incidence angle and the first section of the model is observed to have a negative pathloss. Time-of-arrival (TOA) of the first path has been modeled as a two-section model as well with the same break point used in the pathloss model of the first path. The total pathloss has very

TABLE I
SPECIFICATION OF VNA AND ANTENNA

Parameters	Values
VNA	Agilent E8363
Frequency Range	3-8 GHz
Sample point number	1601
Calibration	Responese
Transmit power (P_{Tx})	0 dBm
IF Bandwidth	3 KHz
Antenna	Skycross SMT-3TO10M

similar trend with the pathloss of the first path so that they are modeled by the same equation with different coefficients. The empirical model presented in this paper illustrates the behavior of RF waveform when passing the human body and can be regarded as the theoretical basis of the further development of the ray-tracing technique with human body taken into consideration.

The remainder of this paper is organized as follows. In Section II, brief description of the measurement setup and scenario has been provided. In Section III, we model the power of the first path, first path TOA and the total power of the near body UWB channel. In Section IV, conclusion of this paper and discussion of the future works are presented.

II. MEASUREMENT SETUP AND SCENARIO

The empirical measurements are performed in the frequency band ranging from 3GHz to 8GHz in an anechoic chamber. The methodology of data collection will be discussed in detail in this section.

A. Measurement setup

The measurement system employed in this paper consists of a vector network analyzer (VNA, Agilent E8363), a pair of low loss cable, a 30dB power amplifier and a pair of small size UWB patch antenna (Skycross SMT-3TO10M). The power amplifier is employed to guarantee the peak detection at the Rx side due to the huge pathloss of the near body channel. A medium size male remaining standing posture is selected as the objective of the measurement. The Tx atenna has been attach to the middle of the human chest at the height of 1.29m while the Rx antenna is tied to a tripod of the same height. Since the antenna-body interaction is an integral part of the overall propagation characteristic, the influence of antenna has been included as a part of our model. Parameters used in VNA calibration are listed in Table 1 and system components are connected as is depicted in Fig. 1.

The S parameter S_{21}, which is also known as the channel transfer function has been measured by the VNA in frequency domain. The recorded spectrum profile $Y(\omega)$ is given by:

$$Y(\omega) = H(\omega)X(\omega) + N(\omega) \tag{1}$$

where $H(\omega)$ represents the channel impulse response and $N(\omega)$ represents the addictive white Gaussian noise (AWGN), respectively [8]. A symmetric hamming window has been applied to the frequency domain at the cost of time resolution in order to limit the sidelobe and enable detection of more multipath component. The hamming window is given by:

$$\omega(n) = \begin{cases} 0.54 - 0.46\cos(\frac{2\pi n}{N}), & 0 \le n \le N \\ 0, & \text{otherwise} \end{cases} \tag{2}$$

The frequency domain profile is transferred to time domain by a base band complex inverse fast Fourier transform (IFFT). Typical recorded time domain channel profile has been shown in Fig. 2 in which proper threshold has been established to detect the first path, thus determine the first path pathloss and first path TOA.

B. Measurement scenario

From the perspective of scenario-based approach, a measurement case set denoted by:

$$Case = \{\theta, d\}$$

is composed of a subset θ which is the incidence angle of rays and subset d which is the distance between Tx and Rx. A

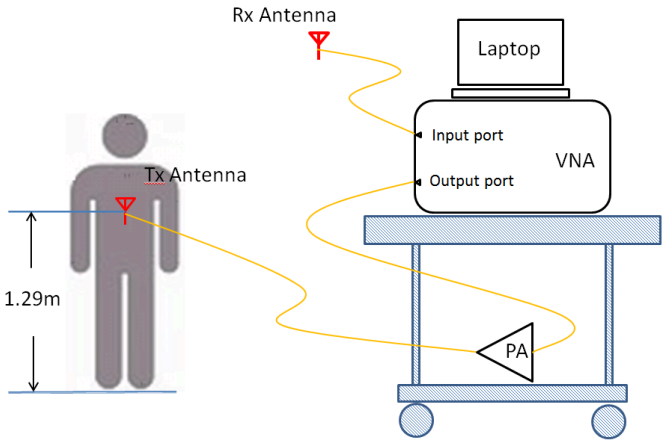

Fig. 1. Sketch of the UWB measurement system.

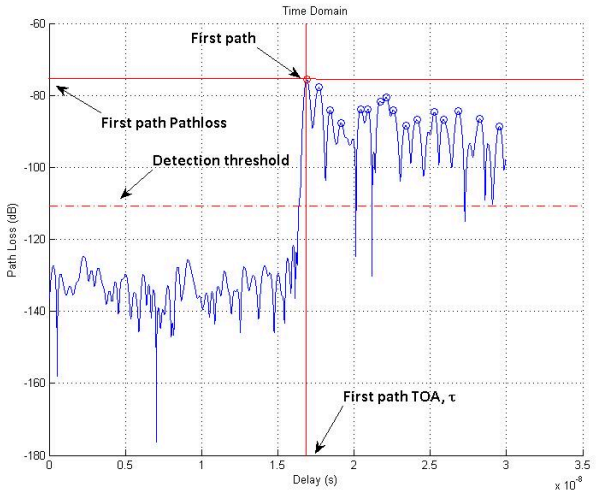

Fig. 2. Sample time domain channel profile with detection threshold.

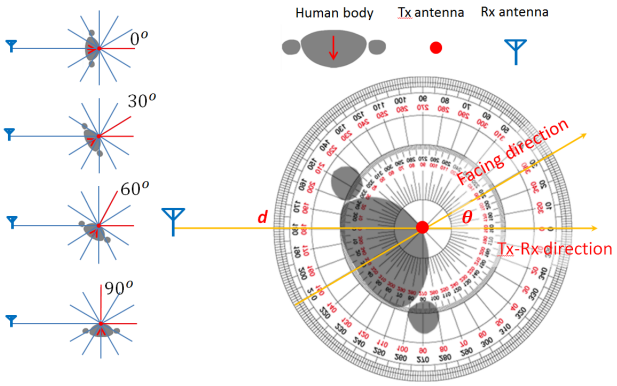

Fig. 3. Definition of incidence angle θ and Tx-Rx distance d.

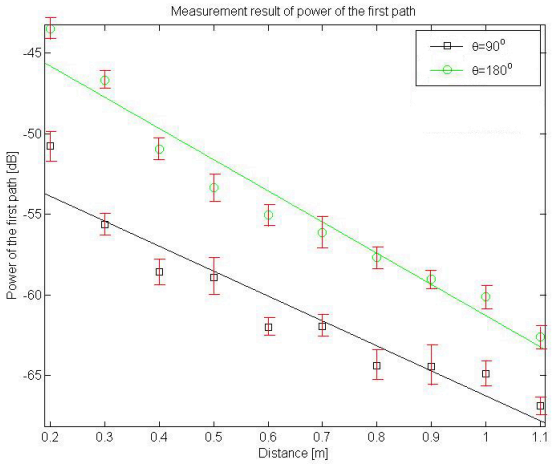

Fig. 4. First path pathloss in LOS scenario and 90^o case of NLOS scenario

specific case of our measurement can be $Case = \{30^o, 0.6m\}$. Over 300 snapshots are obtained in each case to guarantee the validity of the near body model.

1) Incidence angle θ: The Incidence angle is defined as the horizontal angle between human facing direction and the direction of Tx-Rx. Fig. 3 shows the torso section extracted from 3D scan of our measurement objective. It is at the same height of Tx antenna which is 1.29m. The section is then attached to a protractor plane and a 30^o sample incidence angle can be seen clearly. The measurements are performed every 30^o so that the subset θ is given by:

$$\theta = \{0^o, 30^o, 60^o, 90^o, 120^o, 150^o, 180^o\}$$

The measurement cases are also partitioned into line-of-sight (LOS) and non-line-of-sight (NLOS) scenarios by whether the human body is blocking direct line between Tx and Rx. To help classify these two scenarios, we define the relationship between incidence angle θ and physical scenario S as:

$$S = \begin{cases} NLOS, & \theta \in [0^o, 90^o] \\ LOS, & \theta \in (90^o, 180^o] \end{cases} \quad (3)$$

2) Tx-Rx distance d: Since the RF waveform travels as creeping wave along the surface of human body, one possible approach is to define d as the actual travel distance which is the combination of both on-body creeping distance and off-body propagation distance. However, to facilitate the modeling process, we define the Tx-Rx distance d as the straight-line distance between Tx and Rx.

The definition of d can be also seen in Fig. 3. Throughout the measurements, both the locations of Tx antenna and the Tx-Rx direction are fixed and the variation of incidence angle θ is achieved by changing the standing position and facing direction of the objective. For each incidence angle θ, the Rx antenna has been initially located at the minimum possible distance $d_{0,\theta}$ and then moved away from human body for every 10cm along the Tx-Rx direction. The maximum distance between Tx and Rx is limited within 1.1m so that the distance subset can be given by:

$$d = \{d_{0,\theta}, 30\text{cm}, 40\text{cm}, 50\text{cm}, ..., 100\text{cm}, 110\text{cm}\}$$

In LOS scenario and the 90^o case of NLOS scenario, existence of human body does not hinder the Rx antenna set up so that we let $d_{0,\theta} = \{10cm, 20cm\}$. In rest of the NLOS scenario, minimum possible initial distance $d_{0,\theta}$ is the intersection point of body surface and Tx-Rx direction. Since it depends on the size and shape of human body involved in the measurement, we calculated the $d_{0,\theta}$ on the torso section and listed the values of $d_{0,\theta}$ in table II.

III. Empirical Channel Model

In this section, we first discuss the propagation characteristic of the near body UWB channel separately in LOS and NLOS scenario and then provide an general model for both scenarios.

A. First Path Pathloss

1) LOS scenario: Empirical measurement result shows that, in LOS scenario, the first path pathloss is independent to the incidence angle θ so that we calculate the mean and variance of measurement results for each Tx-Rx distance d in the subset and plot them in Fig. 4. As can be seen from the linear regression fitting result in Fig. 4, the first path pathloss $P_{first}(d)$ can be modeled as a linear function of d:

$$P_{first}(d) = L_{0,\text{LOS}} + 10\alpha_{1,\text{LOS}} \log_{10}(d) + S_{\text{LOS}} \quad (4)$$

where d is the Tx-Rx distance defined in previous section, $L_{0,\text{LOS}}$ denotes to the pathloss at reference distance of 0 mm, $\alpha_{1,\text{LOS}}$ is the pathloss exponent representing the fading rate and S_{LOS} denotes to the fluctuation term of the first path pathloss in LOS scenario.

2) NLOS scenario: The measurement results of 90^o case in NLOS scenario has been also depicted in Fig. 4. In that case, the first path pathloss can be also modeled as a linear function of d with very similar fading rate ($\alpha_{1,90^o}$) but different pathloss at reference distance ($L_{0,90^o}$) compared with LOS scenario. The model of 90^o case in NLOS scenario is given by:

$$P_{first}(d) = L_{0,90^o} + 10\alpha_{1,90^o} \log_{10}(d) + S_{90^o} \quad (5)$$

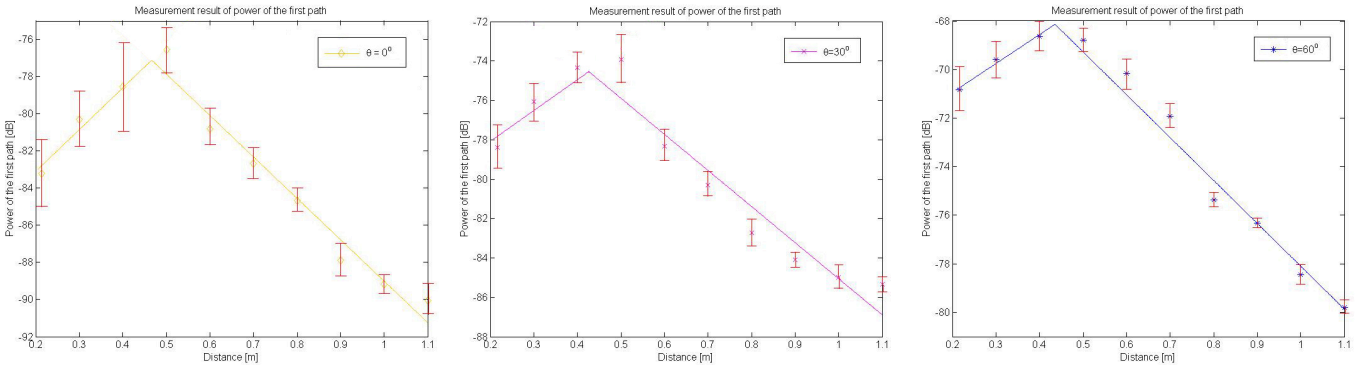

(a) (b) (c)

Fig. 5. First path pathloss in NLOS scenario. (a): $\theta = 0^o$. (b): $\theta = 30^o$. (c): $\theta = 60^o$.

An approximately 8dB bias between $L_{0,90^o}$ and $L_{0,\text{LOS}}$ can be seen from Fig. 4, which is caused by the effect of human body in 90^o case.

As for the rest of cases in NLOS scenario, the signal strength of detected first path has been shown in Fig 5.(a) (b) and (c). Three observation can be brought about from the empirical measurement results: 1) pathloss of the first path has been partitioned into two sections by a distance break point. The break point is between 0.4 and 0.5m; 2) In the first section, a negative increase on first path pathloss can be observed while in the second section, it becomes positive increase; 3) The range of fluctuation of first path pathloss in the first section is much larger than that of the second section.

Reasonable explaination can be made for the above mentioned observations. Fig. 6 sketched the near body propagation route that RF signal travels along. Waveforms start from the Tx antenna, creep to the other side of human body along the body surface and then get scattered at specific point. The the scatter point serve as another antenna and the scattered waveforms continue propagating in free space and finally reach the Rx antenna. As a result, with the increment of Tx-Rx distance, the creeping distance decreases while the free space propagation distance increases. According to the distance based UWB on body model proposed in [7], the on body signals get much more attenuation per unit distance compared with the signal in free space, so that creeping phenomenon is dominating the pathloss of first section while the free space propagation masters the pathloss of second section. Based on the analysis, we define the first section as on-body section and second section as off-body section. The alternation of effects of two phenomenons takes place at the break point and the larger fluctuation of on-body section also has an agreement with [7].

Since each of the two sections has a linear trend individually, the overall pathloss of the first path can be modeled as:

$$P_{first}(d) = L_{0,\theta} + \begin{cases} 10\alpha_{1,\theta}\log_{10}(d) + S_{\text{on-body},\theta}, & d \le d_{bp,\theta} \\ 10\alpha_{1,\theta}\log_{10}(d_{bp,\theta}) & \\ \quad +10\alpha_{2,\theta}\log_{10}(d/d_{bp,\theta}) + S_{\text{off-body},\theta}, & d > d_{bp,\theta} \end{cases} \tag{6}$$

where $d_{bp,\theta}$ is the distance break point, $\alpha_{1,\theta}$ and $\alpha_{2,\theta}$ denote to the pathloss exponent that determine the fading rate in each section, $S_{\text{on-body}}$ and $S_{\text{off-body}}$ are fluctuation terms, and $L_{0,\theta}$ denotes to pathloss at the reference distance of 0mm again. All of the coefficients in this model are related to incidence angle θ.

3) General model: When $d \le d_{bp}$, the pattern of equation (6) is identical to equation (4) and (5) so that given infinity d_{bp} in LOS scenario and 90^o case of NLOS scenario, equation (6) can be used to uniformly represent the first path pathloss. Values of all these coefficients are listed in table II.

B. First Path TOA

Another important aspect in designing the ray-tracing technology considering the effects of human body is the arrival time of first path. That aspect is especially important for TOA based localization applications. To get a better understanding on the effects of human body on first path TOA, we plot the empirical result for all measurement cases in Fig. 7.

1) LOS scenario: Fig. 7 shows that, in LOS scenario, the first path TOA is a linear function of Tx-Rx distance d which can be modeled as

$$\tau(d) = \gamma_{\text{LOS}}(d) + \delta_{\text{LOS}} \tag{7}$$

where $\tau(d)$ represents the first path TOA, γ_{LOS} denotes to the velocity of first path in LOS scenario and δ_{LOS} represents the delay caused by human body. By comparing the empirical

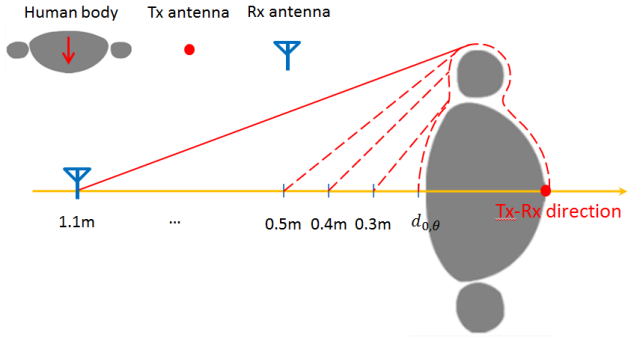

Fig. 6. Sketch of the propagation route from Tx to Rx.

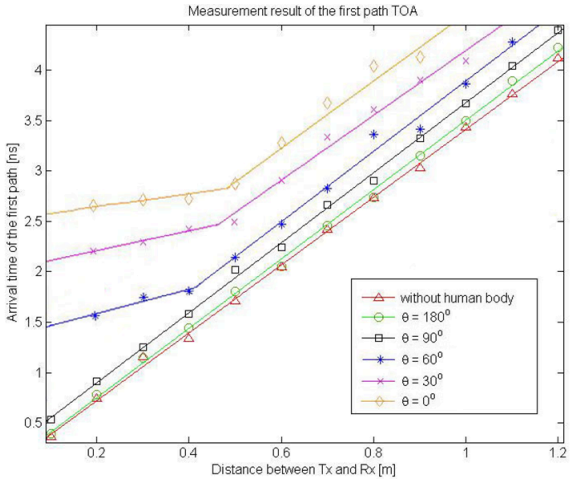

Fig. 7. First path TOA in all measurement cases.

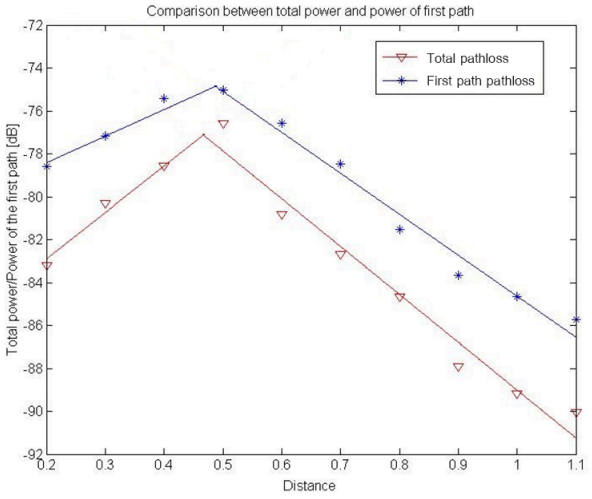

Fig. 8. Comparison between first path pathloss and total pathloss, $\theta = 0^o$.

measurement results with the free space propagation characteristics, a negligible 0.065ns bias can be observed in LOS scenario.

2) NLOS scenario: Same situation happens in the 90^o case in NLOS scenario. There is no creeping distance in that case so that the first path TOA is still linear. However, the bias caused by human body goes up to 0.2ns and the first path TOA for 90^o case is given by:

$$\tau(d) = \gamma_{90^o}(d) + \delta_{90^o} \tag{8}$$

where γ_{90^o} denotes to the velocity of 90^o case in NLOS scenario and δ_{90^o} represents the bias with free space propagation.

As for $0^o, 30^o$ and 60^o cases in the NLOS scenario, the model of first path TOA can be also partitioned into two sections in the same way as the first path pathloss model. Our empirical measurement results in Fig.7 shows that the break points for each incidence angle θ is also identical to the first path pathloss model. In the on-body section, the first path TOA has a smaller velocity compared with free space velocity because the the actual creeping distance for the on-body section is longer than the straight-line distance employed in the model. However, in off-body section, the velocity of waveform is almost the same as free space propagation when the actual propagation distance becomes very close to the straight-line distance. One thing also worth mentioning is that in the angle based on body UWB model proposed by [9], first path TOA is modeled as $\tau(\theta) = \frac{\theta\pi}{360} + \Delta t$, indicating an approximately 5ns delay for every 30^o difference in the incidence angle. Fig. 7 shows that in the on-body section, the bias between two neighboring measurement cases has a close agreement with the model in [9] while in the off-body section, the bias is smaller. Such agreement also proves the validity of the physical process described in Fig. 6.

Based on above analysis, the first path TOA in these cases can be modeled as:

$$\tau(d) = \begin{cases} \gamma_{\text{on-body},\theta}(d) + \delta_{\text{on-body},\theta}, & d \le d_{bp,\theta} \\ \gamma_{\text{off-body},\theta}(d) + \delta_{\text{off-body},\theta}, & d > d_{bp,\theta} \end{cases} \tag{9}$$

where the $\gamma_{\text{on-body},\theta}$ and $\gamma_{\text{off-body},\theta}$ represents the velocity of waveform for on-body and off-body section and $\delta_{\text{on-body}}$ and $\delta_{\text{off-body}}$ represents the time delay caused by human body.

3) General model: Similar with the the model for first path pathloss, the first path TOA model for LOS scenario and 90^o case in NLOS scenario can be merged into the a general model due to the fact that equation (7) (8) and (9) share the same pattern. The general model is given by:

$$\tau(d) = \begin{cases} \gamma_{\text{off-body},\theta}(d) + \delta_{\text{off-body},\theta}, & \theta \in (90^o, 180^o] \\ \gamma_{\text{on-body},\theta}(d) + \delta_{\text{on-body},\theta}, & \theta \in [0^o, 90^o], d \le d_{bp,\theta} \\ \gamma_{\text{off-body},\theta}(d) + \delta_{\text{off-body},\theta}, & \theta \in [0^o, 90^o], d > d_{bp,\theta} \end{cases} \tag{10}$$

where $\tau(d)$ represents the first path TOA, d_{bp} denotes to the distance break point, $\gamma_{\text{on-body},\theta}$ and $\gamma_{\text{off-body},\theta}$ represents the velocity of RF signal and $\delta_{\text{on-body},\theta}$ and $\delta_{\text{off-body},\theta}$ represents the bias from free space propagation. All these coefficients are related to the incidence angle θ and for 90^o case in NLOS scenario, the d_{bp} is set to infinity.

C. Total Pathloss

The total pathloss is obtained from an approach that is different from the first path pathloss and first path TOA. Since the total pathloss is the integration of pathloss on the whole frequency band, instead of recording the time domain channel profile, we abtained the total path according to the following equation:

$$P_{total}(d) = -20\log_{10}\left(\frac{1}{N_s}\frac{1}{N_f}\sum_{i=1}^{N_s}\sum_{n=1}^{N_f}|H_i^p(n)|\right) \tag{11}$$

where $P_{total}(d)$ is the total pathloss at distance d, N_s is the number of snapshots which is 300 in this paper, N_f is the number of frequency sample points in each snapshot which is 1601 and $H_i^p(n)$ is the S_{21} reading at each sample point from the VNA.

Sample measurement results of the total pathloss has been depicted in Fig. 8 for which the incidence angle $\theta = 0^o$. The

TABLE II
COEFFICIENTS FOR THE NEAR BODY UWB MODEL.

θ	d_0	d_{bp}	First path pathloss					First path TOA				Total pathloss				
			$L_{0,\theta}$	$\alpha_{1,\theta}$	$\alpha_{2,\theta}$	$S_{\text{on-body},\theta}$	$S_{\text{off-body},\theta}$	$\gamma_{\text{on-body},\theta}$	$\gamma_{\text{off-body},\theta}$	$\delta_{\text{on-body},\theta}$	$\delta_{\text{off-body},\theta}$	$L_{0,\theta}$	$\beta_{\text{on-body},\theta}$	$\beta_{\text{off-body},\theta}$	$S_{\text{on-body},\theta}$	$S_{\text{off-body},\theta}$
0	0.2134	0.497	71.34	-1.757	4.022	3.1750	0.9814	0.656	3.345	1.225	2.521	72.03	-0.943	3.237	3.0252	0.8751
30	0.1927	0.463	69.74	-1.259	3.167	2.3146	0.8947	0.842	3.331	0.994	2.042	70.43	-0.723	1.902	2.1902	0.8324
60	0.2164	0.411	65.32	-0.926	2.194	1.2615	0.5250	0.997	3.314	0.419	1.532	65.96	-0.598	1.798	1.2957	0.6553
90	10, 20	inf	65.75	2.081	NA	0.4742	NA	NA	3.341	NA	0.204	64.87	2.125	NA	0.4551	NA
LOS	10, 20	inf	60.46	2.485	NA	0.3934	NA	NA	3.347	NA	0.065	60.02	2.329	NA	0.3356	NA

distance break point is still identical to the first path pathloss model. From the figure we see that for each distance, although most of the energy condensed on the first path, the total power at the receiver side is still higher than the power of the first path. In both on-body and off-body sections, we also observed more gentle change on the total power compared with the power of first path and minimum bias between total power and power of the first path occurs at the break point.

According to the similar approach in deriving the first path pathloss model, the total pathloss of near body UWB channel can be given as:

$$P_{total}(d) = L_{0,\theta} + \begin{cases} 10\beta_{1,\theta}\log_{10}(d) + S_{\text{on-body},\theta}, & d \le d_{bp,\theta} \\ 10\beta_{1,\theta}\log_{10}(d_{bp,\theta}) & \\ \quad +10\beta_{2,\theta}\log_{10}(d/d_{bp,\theta}) + S_{\text{off-body},\theta}, & d > d_{bp,\theta} \end{cases} \tag{12}$$

where $P_{total}(d)$ represents the total pathloss for near body UWB channel, $d_{bp,\theta}$ is the same distance break point as previous models, $\beta_{1,\theta}$ and $\beta_{2,\theta}$ denotes to the fading rate and $S_{\text{on-body},\theta}$ and $S_{\text{off-body},\theta}$ is the fluctuation term. $d_{bp,\theta}$ for all LOS scenario and the 90^o case in NLOS scenario is infinity and all these coefficients are listed in table II.

IV. CONCLUSION

In this paper, a near body UWB channel model has been built based on empirical measurement conducted inside an anechoic chamber. The frequency range of the near body model is from 3GHz to 8GHz, covering most of the UWB band. The near body model concentrates on three critical aspects of propagation characteristics which are first path pathloss, first path TOA and total pathloss. All these aspects have been partitioned into on-body section and off-body section based on whether the creeping phenomenon or the free space propagation is dominating the characteristics of the channel. The purpose of creating the near body channel model is to enable the development of ray-tracing technology that can take the effect of human body into consideration. Such model will further facilitate the advancement of wireless access and localization due to the fact that cells are becoming smaller and BAN will take over the attention of both academic and industry at last.

As for future work, we plan to repeat all the measurements in finite difference time domain (FDTD) software simulation to validate the near body model. Apart from that, except for the human chest, on body sensors are often located on human wrist, waist, ankle or inside trouser pocket. According to the analysis in this paper, we infer that the near body model also depends on the location of on body sensor so that related research is still in demand. The next step is to merge the near body model into the channel model between body surface and external access point and we may try to update our ray-tracing software by designing human body module for it.

ACKNOWLEDGMENT

The authors would like to thank Mao Wenbo from Wake Forest University and Adria Fung from WPI for editing the paper and Dr. Yunxing Ye from CWINS, WPI for building the measurement system. This work has been performed under the American Recovery and Reinvestment Act Measurement, Science and Engineering Grants program (NIST Grant No. 60NANB10D001), which is sponsored by the National Institute of Standards and Technology (NIST). This work is also supported by Wireless Health Monitoring and Location Tracking, Rapid Product Development Center (UCLA subcontract No. 1562-S-PD386), which is sponsored by US Department of Interior/DHS. This work is partly supported by the National Natural Science Foundation of China (Grants No. 61003251 and No.61172049).

REFERENCES

[1] D. Cassioli, M.Z. Win and A.F. Molisch, The ultra-wide bandwidth indoor channel: from statistical model to simulations, *IEEE journal on selected areas in communications*, pp.1247-1257, Vol.20, Issue.6, 2002.

[2] A.F. Molisch, J.R. Foerster and M. pendergrass, Channel models for ultrawideband personal area networks, *IEEE wireless communications magazine*, pp.14-21, Vol.10, Issue.6, 2003.

[3] IEEE, 802.15 Tg6 ,Draft of Channel Model for Body Area Network, November, 2010.

[4] M. Hassan-Ali and K. Pahlavan, Site-specific wideband indoor channel modelling using ray-tracing software, *IET Electronics Letters*, pp.1983-1984, Vol.33, Issue.23, 1997.

[5] J. He, S. Li, K. Pahlavan and Q. Wang, A Realtime Testbed for Performance Evaluation of Indoor TOA Location System, *IEEE International Conference on Communications (ICC)*, Ottawa, Canada Jun. 2012.

[6] J. He, Y. Geng and K. Pahlavan, Modeling indoor TOA Ranging Error for Body Mounted Sensors, *2012 IEEE 23nd International Symposium on Personal Indoor and Mobile Radio Communications (PIMRC)*, Sydney, Australia Sep. 2012

[7] A. Fort, C. Desset, J. Ryckaert, P.D. Doncker, L.V. Biesen and P. Wambacq, Characterization of the ultra wideband body area propagation channel, *2005 IEEE International Conference on Ultra-Wideband*, Zurich, Switzerland Sep. 2005

[8] X. Chen, X. Lu, D. Jin, L. Su and L. Zeng, Channel Modeling of UWB-Based Wireless Body Area Networks, *2011 IEEE International Conference on Communications*, Kyoto, Japan Jun. 2011

[9] J. Chen, Y. Ye and K. Pahlavan, UWB Characteristics of Creeping Wave for RF Localization Around the Human Body, *2012 IEEE 23nd International Symposium on Personal Indoor and Mobile Radio Communications (PIMRC)*, Sydney, Australia Sep. 2012